Tunneling hot carrier transistors

Stijn Goossens
(a.m.goossens@student.rug.nl)
11 June 2007
Zernike Institute for Advanced Materials, Groningen, The Netherlands

Tunneling hot carrier transistors are part of a novel family of three terminal hot carrier amplifiers. High speed performance is predicted for these devices. Although the idea originates from the sixties, there is still much to do to improve the performance of the hot carrier transistors.

The principles of operation of the transistors are explained and the most important loss mechanisms are reviewed. Also the requirements for the operation of the transistors in electronic circuits are evaluated.

There are many ways to fabricate the tunneling hot carrier transistor. Metal base transistors have been made, but also heterojunction monolithic semiconductor hot carrier transistors. An overview is given of all different THCTs. Design considerations are reviewed and experimental results are compared.

In most devices poor fabrication is the bottleneck of performance. As production technology developed, better devices were made, but they are still not good enough to rival conventional transistors. Frequency performance is only measured for a few monolithic semiconductor devices with a maximum current gain cut-off frequency of 121 GHz. Recently developed polymer hot carrier transistors show one of the highest common emitter gains of 41 at room temperature.

1 Introduction

In the ongoing search for faster electronic circuits the main focus was downscaling of device size. Further miniaturizing conventional semiconductor devices would dramatically increase their resistance. Another disadvantage of conventional semiconductor devices is their horizontal topography. They are manufactured using UV-lithography or maybe even E-beam lithography, but a resolution smaller than 10 nm seems impossible. A logic change in device topography would be to go vertical. When evaporating techniques are used, layer thickness can be controlled up to the lattice parameter length scale.

As the storage time of minority carriers is a speed limitation in a conventional bipolar transistor, a unipolar device would be an improvement. The transport mechanism in conventional transistors is diffusion, so the use of high velocity carriers could be another solution in the search for speed. A device structure that incorporates vertical topography, unipolarity and high velocity carriers is the tunneling hot carrier transistor (THCT), first proposed by C.A. Mead in 1960 [10]. In this device a tunneling barrier is used as an electron launcher that abruptly accelerates the tunneling electrons from the emitter to the base.

Tunneling is a very fast process, as resonant tunneling through quantum wells up to 2,5 THz [41] and oscillation frequencies of tunnel barriers up to 700 GHz have been observed [46]. Part of the hot quasi mono-energetic hot electron beam injected in the base of the transistor is observed to traverse the base balistically [2].

Tunneling hot carrier transistors are not only useful devices for high speed electronic applications, but also for hot electron transport spectroscopy [2] and application in spin transport devices as spin of an electron is conserved while tunneling [51]. Another nice feature of THCTs is the occurrence of negative differential resistance, an effect that can be used to make logic circuits with very few components.

One should pay attention to the fact that THCTs are a kind of hot carrier transistor. There are also hot carrier transistors that inject hot carriers by thermionic emission. To get insight in the family of hot carrier transistors, Fig. 1 is a schematic overview of different device structures.

In this paper, hot electron transistors with tunneling injection are reviewed. The thermionic injection hot electron transistors have promising high frequency performance too, but are beyond the scope of this article. For convenience, the names of the authors that worked on thermionic injection devices are mentioned in the diagram.

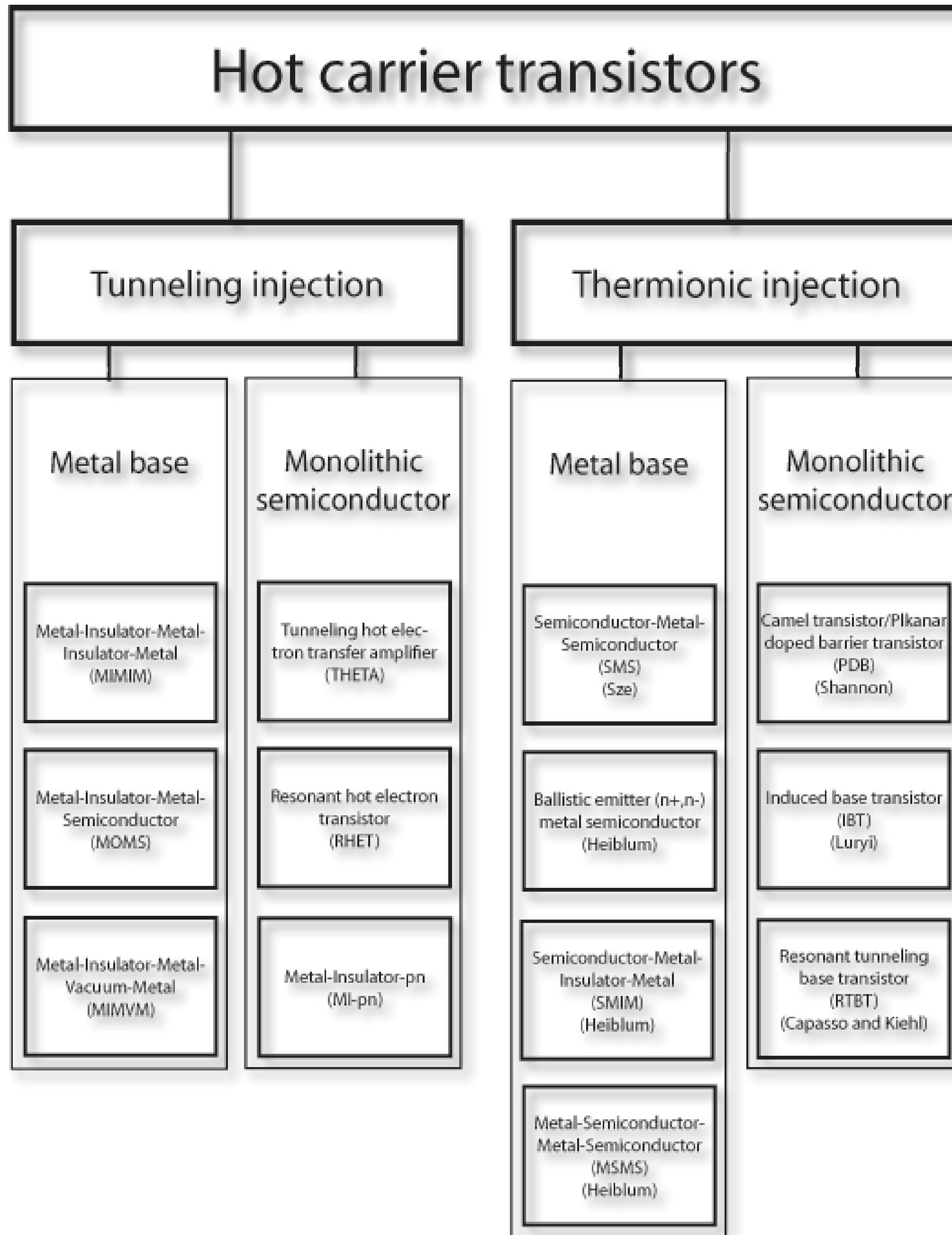

Fig. 1 *Diagram of different types of hot carrier transistors*

2 *Principles and concepts*

2.1 Operation principles

A tunneling transistor consists of the same elements as a normal bipolar transistor: emitter, base and collector. The emitter injects a hot electron beam in the base. The electrons in the beam traverse the base and are collected by the collector. What is special about a tunneling transistor is the way it injects electrons into the base, namely by a tunnel junction.

Suppose two metals are connected with a thin energy barrier in between, this is called a tunnel junction. If the electric field in the barrier is high enough, the electrons have a certain probability to be transported to the other side of the barrier. This generates a net tunneling current. In a tunneling transistor a tunnel junction is used to inject hot electrons. In Fig. 2a a schematic layout of a tunnel transistor is shown. The tunnel junction consists of two metal layers (emitter and base) and an insulator layer that functions as an energy barrier in between. If a positive bias V_{BE} is applied to the base, a net tunneling current flows from the emitter into the base, as is shown in the energy diagram Fig. 2b.

The tunnel current generates a beam of electrons with an energy distribution around E_{FE} (Fermi energy of the emitter) in the base. This beam consists of hot electrons: electrons with an energy more than a few kT higher than the Fermi level. (This in contrast with ‘cold’ electrons, electrons which have an energy comparable to the Fermi energy). To minimize the number of ‘cold’ electrons flowing from the base to the collector, a broad barrier between the base and collector is required (as can be seen in Fig. 2b) .

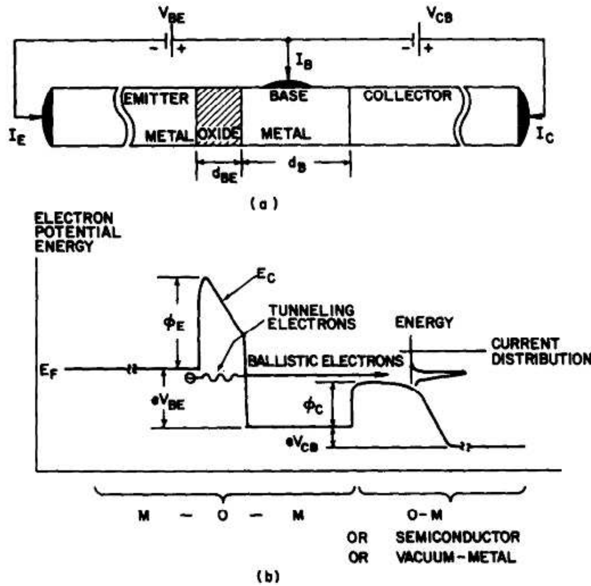

Fig. 2 a) General layout of a tunnel transistor, a one dimensional model applies since the linear dimensions are much smaller than the other dimensions b) Energy diagram of the tunnel transistor with image force corrected barriers [1]

A bias V_{CB} accelerates the hot electrons to the collector and if the base is thin enough and the electrons have an energy high enough to pass the base-collector barrier Φ_C, the electrons can flow into the collector. With this last element, a three terminal device is completed.

If $V_{BE}< \Phi_C/e$ the hot electrons bounce back off the base-collector barrier and are thermalized in the base, resulting in I_E=-I_B. Biasing the collector positively (V_{CB}>0) will leave the barrier height unaffected (neglecting the image charge correction) and the observed collector current will result only from tunneling electrons from the base.

The collector current will suddenly rise when V_{BE} exceeds Φ_C/e - δ, provided the energy distribution of the tunneling electrons is characterized by δ, half the normal energy spread of the electron beam energy distribution. The input power for switching the output of the device in common base configuration will be small (directly proportional to δ^2, which is temperature and parameter sensitive).

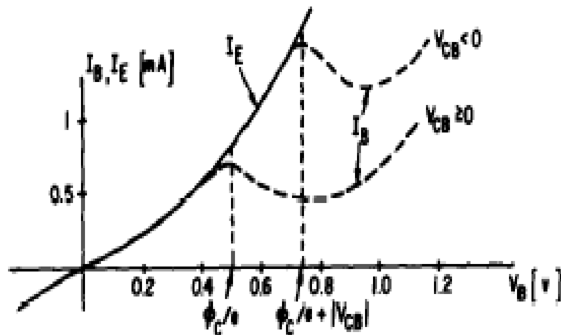

Fig. 3 I_B vs V_{BE} shows negative differential resistance (NDR) [1]

If the tunnel transistor is operated in common emitter configuration, negative differential resistance should be observed. This effect is shown in Fig. 3: when V_{BE} exceeds Φ_C/e, so when the transistor is turned "ON", I_B decreases with increasing V_{BE}. The onset of negative differential resistance can be controlled by V_{CB} [1].

For normal bipolar transistors the gain in common emitter configuration is an important figure of merit. The common emitter gain is defined by β= I_C/I_B. For bipolar transistors the common emitter gain is related to the transfer ratio by β = α/(1- α). In some publications on hot carrier transistors, this relation is used to calculate the transfer ratio of the device. In reference [39] it is observed that the relation does not hold for their tunnel transistor. The tunneling current responds to biases differently than the diffusion current in bipolar transistors. This occurs because hot electron transport, particular resonant tunneling, is a highly nonequilibrium process. Transistor modeling should include the hot electron relaxation process. In this paper the relation between α and β is used, but if it's used, the common emitter current β gain is stated.

2.2 Loss mechanisms

Due to loss processes, only part of the injected emitter current (I_E) is collected by the collector. This leads us to define the transfer ratio α=-I_C/I_E, using the convention of I>0 when it flows into the port and I_C the collector current. (notice that α is also referred to as the 'common base' current gain).

2.2.1 Quantum mechanical spread of tunneling electron current

The tunnel barrier injects hot electrons in the base. When the barrier is thin enough, a substantial flow of electrons is permitted if the effective barrier height is lowered by applying a bias V_{EB}.

According to Heiblum and Fischetti [2] the current density through the tunnel barrier can be calculated by the following equation:

$$J(V) \cong \frac{e}{2}\int_0^\infty dE \frac{\rho(E) f(E)[1-f(E+eV)]}{[2m_{en}(E)E]^{1/2}} \times \int_0^E dE_n T(E_n, V)$$

With f(E) the cathode Fermi function, m_{en} the "energy effective mass" [3], E_n the energy normal to the barrier and T(E_n, V) the transmission probability.

Now, the following three distributions can be defined, a total energy distribution D_{tot}(E,V), a normal energy distribution D_{norm}(E_n,V) and an angular distribution D_{ang}(θ,V):

$$J(V) = e\int_0^\infty dE D_{tot}(E,V)$$

$$J(V) = e\int_0^\infty dE_n D_{norm}(E_n,V)$$

$$J(V) = e\int_0^{\pi/2} d\theta D_{ang}(\theta,V)$$

These distributions have been calculated numerically by Heiblum for a metal base tunnel transistor [1] and a monolithic semiconductor tunnel transistor [2]. As an example, the calculated normal current distribution of a metal base tunnel transistor for a barrier height of Φ_E=0.7 eV and an emitter barrier thickness of 15 Å is plotted in Fig. 4.

In Table 1 the calculated peak positions of the normal (a) and total energy distributions (b) of a 2 eV barrier (Φ_E=2 eV is a realistic value for the barrier height of an Al-Al_2O_3-Al junction.) and of the normal energy distribution of a 0.7 eV barrier are summarized. Important features in the table are the following: the distribution peak is not situated exactly at the Fermi energy and shifts up in energy until eV= Φ, a further increase in V (entering the Fowler-Nordheim tunneling regime) causes the peak to shift down. For biasing values of $eV_{BE} >\approx \Phi_E$, the narrowest and least displaced energy distribution is obtained. The narrowest energy distribution will possibly result in the highest transfer ratio, because it is easier to optimise the collector bias

No results are plotted for the angular distribution function. The important result of the calculation of this distribution is that only a small number of electrons will approach the barrier at zero angle, so the maximum current through the barrier will be due to electrons with a small, but nonzero angle.

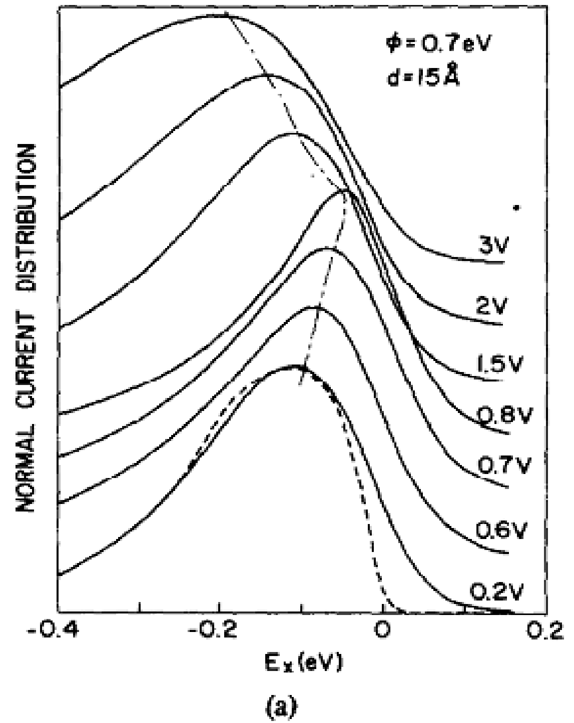

Fig. 4 Normal current distribution of a metal base tunnel transistor as a function of energy normal to the barrier for different biasing conditions, barrier thickness 15 Å and Φ_{BE} 0.7 eV. [1]

d[Å] \ V[v]	0.5		1.5		2		3		5	
10	.07	.3	.06	.29	.05	.26	.056	.24	.075	.34
25	.035	.17	.023	.15	.015	.15	.023	.14	.038	.18
50	.003	.14	-.012	.14	-.058	.26	-.012	.14	.015	.14

(a) φ = 2eV: TOTAL CURRENT DISTRIBUTIONS

d[Å] \ V[v]	0.5		1.5		2		2.5		3		6	
10	.15	.51	.11	.65	.06	.56	.06	.43	.1	.51	.2	.8
25	.10	.27	.077	.23	.05	.22	.053	.18	.073	.22	.14	.4
50	.03	.17	.017	.17	-.045	.30	.0	.23	.017	.16	.075	.2

(b) φ = 2eV: NORMAL CURRENT DISTRIBUTIONS

d[Å] \ V[v]	0.2		0.6		0.7		0.8		1.5		2		3	
15	.104	.29	.075	.24	.07	.24	.04	.19	.104	.26	.137	.33	.183	.43
20	.08	.21	.054	.22	.042	.22			.087	.22	.121	.29	.17	.37
25	.054	.19	.31	.19			.008	.16	.05	.22	.081	.18	.012	.30

(c) φ = 0.7eV: NORMAL CURRENT DISTRIBUTIONS

Table 1 Peak position on the left and full width at half maximum on the right for a 2 eV and 0.7 eV barrier height at different biasing conditions for different barrier thicknesses. [1]

2.2.2 Spread of tunneling current due to electronic collisions in the conduction band of the base emitter barrier

If the emitter-base barrier is strongly biased ($eV_{BE} > \Phi_E$), tunneling electrons spend part of their path in the conduction band of the emitter. Due to image force correction there are two trajects in this conduction band, one with distance d_{BE}' and one with distance d_{BE}", see Fig. 5. The latter can be neglected, but the former can be a strong scatterer.

In the conduction band of oxides, the mean free path is very short [1]. Scattering will deflect the electrons from the normal direction and this will cause the electrons not being collected. So α will be reduced. For oxide thicknesses in the 100 Å regime and d_{BE}"≈0.3d_{BE} transmission won't exceed 2×10^{-3} if the mean free path in the oxide is about 5 Å [1].

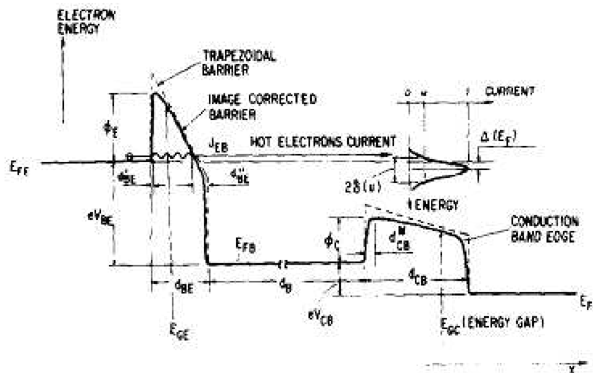

Fig. 5 Detailed band diagram of a tunneling transistor [1]

2.2.3 Scattering of hot electrons in the base

The most important characterization of the transport properties of hot electrons in the base layer is their mean free path: the mean distance an electron can travel without being scattered. (Notice that the mean free path of hot electrons is different from the mean free path that is mentioned in connection with the conductivity of metals.) We should expect the mean free path to decrease with increasing thickness of the layer and can be estimated using the following formula:

$$\alpha = \exp[-d_B / mfp]$$

Where α is the transfer ratio, d_B the width of the base and mfp the mean free path

Heiblum [1] reported mean free paths of at least 100 Å for different metals and varying electron excess energies (see Appendix 1 for the full table). Levi et al. [6] calculated a mean free path of about 300 Å for hot electrons with excess kinetic energy of 250 meV in layers GaAs doped to a level of 1×10^{-18} cm^{-3}.

The scattering mechanisms in metal bases are different than in semiconductor bases. Below the different mechanisms for metals and for semiconductors are outlined shortly:

a) In metals, the mechanisms that influence hot electron scattering are electron-defect or electron-impurity, electron phonon and electron-electron collisions [1]. The electron-defect loss is a permanent loss in the collection process. The mean free path of electron-phonon collisions can be calculated:

$$l_{e-ph} \approx \lambda_\sigma (E_k / E_F)^2$$

λ_σ is the mean free path of thermalized electrons and E_k is the kinetic energy of the hot electrons

The mean free path between electron-electron collisions is dependent on the excess hot electron energy as:

$$l_{e-e} \propto E^{1/2} (E - E_F)^{-2}$$

With E the energy of the hot electrons.

b) In GaAs, the mechanisms that influence the mean free path of hot electrons are electron-electron scattering, optical phonon emission and transfer of electrons to the L-valley [2]. Hollis et al. [7] and Levi et al. [4] have suggested that the dominant scattering mechanism of hot electrons is the scattering due to coupled modes of plasmons and optical phonons.

2.2.4 Quantum mechanical reflection from the base collector barrier interface

Another mechanism that reduces the transfer ratio, is the quantum mechanical reflection of electrons from the base-collector barrier interface. Classically, the electrons are not reflected if their energy exceeds the barrier height. But quantum mechanically, there is always a finite reflection which decreases as the electron excess energy above the barrier increases.

The transmission coefficient of the barrier depends on the shape of the barrier: a rectangular barrier has the highest reflection and the reflection decreases as the barrier gets more graded.

For a simple rectangular barrier, the following expression for reflection is valid [9]:

$$R = \left(\frac{1-\nu}{1+\nu} \right)^2$$

where

$$\nu = \left(1 - \frac{\Phi}{E} \right)^{1/2}$$

Φ is the barrier height and E the electron energy

For a ballistic electron in Al incident on the interface with GaAs at 0.4 eV above the schottky barrier (Φ≈12eV) the probability of reflection is ~50%.

The effective mass on each side of the barrier is also strongly influencing the transmission. The transmission can be expressed as [1]:

$$T = \left(\frac{A_t}{A_i}\right)^2 \frac{m_i^*}{m_t^*}$$

With A the amplitudes of the wave functions, m the effective mass and i and t stand for the medium of incidence and transmission respectively.*

If $m_i^*=m_t^*$ and an excess energy of 0.1-0.4 eV, a reflection of 25% is inevitable.

2.2.5 Transmission through the conduction band of the base-collector oxide

The collector barrier consists of two regions: $x<d^M_{CB}$ en $x> d^M_{CB}$ (see Fig. 5). If the energy of the electron in region $x<d^M_{CB}$ drops below Φ_C the electron will not be collected. On the other hand, if the energy drops below Φ_C in the region $x> d^M_{CB}$ the electron must be collected.

If the energy of the electrons is higher than the barrier height, electrons will pass the barrier. When the energy gets higher and higher, the number of generated optical phonons will increase and the transmission will diminish [1]. If the energy distribution is nearly mono-energetic, maximum transmission will occur at some value of eV_{BE} in the range Φ_C… Φ_C+0.5eV according to Heiblum [1].

2.2.6 QM reflections from the collector oxide- collector interface

Classically, no reflections occur at this boundary, but quantum mechanically they do occur. These reflections only contribute few tens of percents [1].

2.3 Frequency performance

In the first edition of ‘Physics of semiconductor devices’ by S.M. Sze, it is calculated that tunneling injection transistors have a poor frequency performance compared to SMS, bipolar and space charge limited transistors. This could be true for low current densities (in the order of 10^4 A/cm^2). For higher current densities (10^6 A/cm^2), the frequency performance of a tunneling transistor could be better. The experimental results from small area MOM junctions point to a superior performance as a frequency response up to at least the infrared is reported [23],[24].

Luryi [9] disputes the much stated argument that the time of flight across the base allows for subpicosecond operation of hot electron transistors. He states that the characteristic delay times are the transit times through the emitter and collector barrier. These times are given by $\tau_E=l_E/v_{th}$ and $\tau_C=l_C/v_s$, with l_E and l_C the emitter and collector barrier thickness, v_{th} the thermalised electron drift velocity and v_s the saturated electron drift velocity. He thinks an ideally optimized hot electron transistor is roughly a 3 picosecond device.

It is extremely important to have a small area device to reduce the capacitance of the transistor and increase the current density.

3 *Theoretical Design parameters*

In the previous paragraph, all relevant concepts for operation of tunneling hot electron transistors are theoretically reviewed. This paragraph will deal with the practical application of these concepts.

The basic requirement s for operation of a tunneling hot electron transfer amplifier are:

(a) $r_{out}>>r_{in}$ to achieve power gain (r_{out} is the output resistance and r_{in} is the input resistance)

(b) τ_{in} and τ_{out} as small as possible for high frequency performance (τ_{in} is the input transit time and τ_{out} is the output transist time)

(c) maximize α

condition (b) requires small area devices. Small area devices have another advantage: a thin emitter barrier layer is enough to achieve an impedance high enough to overcome problems with the base spreading resistance (this is what the block ‘(5-20) Å oxide thickness convenient resistance’ in Fig. 6 means).

If the collector barrier is low enough (preferably ~0.5 eV), V_{BE} can be small. This has a twofold advantage: 1) operation in the Fowler Nordheim regime can be prevented, which results in a much lower excess energy of the electrons in the base and 2) d_{BE}” is much smaller so scattering in the emitter barrier is reduced. Both result in a higher transfer ratio: requirement (c).

Requirement (a) (high collector impedance) is easily satisfied if $d_{CB} > d_{BE}$.

Fig. 6 summarizes the parameters and performances of a tunneling hot electron transistor, which result from the two basic requirements for practical realisation of tunneling hot electron transistors.

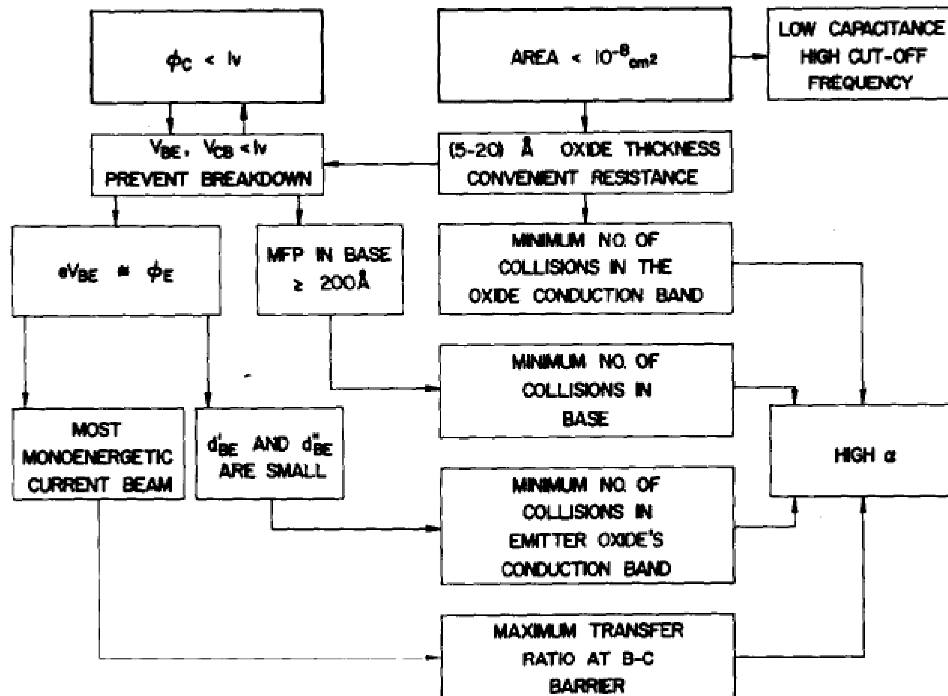

Fig. 6 Diagram of the parameters and performances of a MIMIM. The two basic requirements for the practical realisation are indicated by the heavy line blocks and the final results are the blocks on the right. I_V is the ionisation potential of any of the materials used in the transistor. [1]

4 THCT structures

Before, our attention was mainly focused on a MIMIM (metal-insulator-metal-insulator-metal) transistor, because the principles and concepts that apply to the MIMIM are generally applicable to all tunneling hot carrier transistor structures. As is discussed in the introduction other tunneling hot electron transistors structures possible. There are two main approaches: metal base layer and monolithic semiconductor base layer. Devices with a metal base are the MIMIM, MIMVM and MIMS. Tunneling hot carrier transistors with a monolithic semiconductor base are the THETA, RHET and MI-pn. In this paragraph, I will give an overview of the different tunneling hot carrier devices that have been made in the past. Their structures are reviewed and their performances compared.

4.1 Metal base

4.1.1 MIMVM

The MIMVM (metal insulator metal vacuum metal) uses a MIM tunneling barrier as a hot electron injector and a metal-vacuum-metal barrier as the collector barrier. The hot electrons that are injected have to surmount the workfunction of the base metal to be emitted into the vacuum and collected by the collector.

a) Design considerations

As the workfunction of most stable metals is around 4 eV and the barrier height of a Al-Al_2O_3 barrier is about 2 eV, the MIMVM has to be operated with $eV_{BE}>\Phi_E$, so in the Fowler Nordheim tunneling regime. This results in a high excess energy of the hot electrons, which decreases the mean free path and increases $\Delta(E_F)$ and $\delta(1/2)$ of the current distribution.

Because the emitter oxide has to withstand high operating voltages, the oxide layer has to be thick, which results in a large d_{BE}" and thereby a further increase of $\Delta(E_F)$ and $\delta(1/2)$.

b) Realized devices

In Table 2 paramaters and performances of MIMVMs that are produced in the past are collected.

Up to now MIMVMs are realized as MOMVMs, so with an oxide emitter barrier. As is shown in Table 2, the performance of these MOMVMs is poor. In [18], a metal with a lower workfunction (Ba) was evaporated on top of the base metal (Al) to lower the base-collector barrier, which resulted in a slightly higher transfer ratio.

Table 2 Parameters and performances of past MOMVMs [1]

E-B oxide type	E-B oxide thickness [Å]	Base Metal	Base thickness [Å]	α_{max}	Reference
Al_2O_3	100	Al	100	10^{-3}	[11]
Al_2O_3	75	Al	100	$3x10^{-4}$	[16], [17]
Al_2O_3	67	Al, Al-Ba	100	$<10^{-4}$, $5x10^{-2}$	[18]
Al_2O_3	900	Au	80	$1.8x10^{-2}$	[19]

4.1.2 MIMS

The main problem of the MIMVMs is the high metal-vacuum barrier the electrons have to overcome to be collected. The MIMS (metal-insulator-metal-semiconductor) solves this difficulty by using a semiconductor as the collector material. The semiconductor-metal interface forms a Schottky barrier (Fig. 7) with a much smaller height than the metal vacuum barrier. Most barrier heights are in the range 0.5-1 eV so V_{BE} doesn't have to exceed 1V, which means that the mean free path in the base is larger than 100 Å.

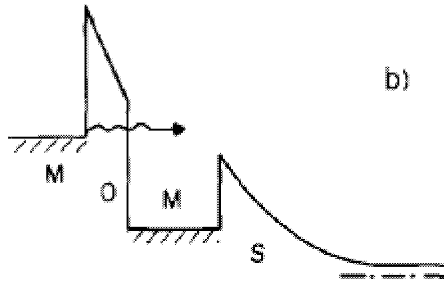

Fig. 7 Schematic band diagram of a MIMS. [9]

a) Design considerations

In a MIMS the barrier height can be adjusted choosing the proper metal semiconductor combination. The main problem of the MIMS is the large depletion layer thickness. This will reduce the transfer ratio and limit the upper operation frequency.

Quantum mechanical reflection and elastic scattering from optical phonons decrease the transmission of electrons to the collector. Crowel and Sze [25] calculated the backscattering of electrons for semiconductor-metal-semiconductor hot electron transistors. They found that the transmission of electrons if fairly constant with the increase of E_e (the minimum total energy of electrons ejected from the emitter) in Si (50-80% reflection) and GaAs (20-50% reflection) depending on the phonon energies. Crowel and Sze calculated reflections of less than 20% for E_x-Φ_C > 0.1 eV, for small m* in the semiconductor. The reflections diminish fast with increasing excess energy of the electrons above the barrier.

If a high electric field is applied across the collector barrier, Φ_C lowers due to the image potential correction. So quantum mechanical reflections decrease, but the probability of multiple phonon creation and backscattering increases.

b) Realized devices

In 1961 James Spratt [5] was the first to report on a working MIMS: a metal-oxide-metal-semiconductor (MOMS) device. The transfer ratio of the device is quite high (0.9), probably due to the unwanted occurrence of pinholes in the evaporated metal base. In reference [20] special care is taken to avoid pinholes and in [21] an extra thick base layer is applied (which immediately reduces the transfer ratio). Heiblum [1] considers the reported high transfer ratio's as questionable.

A very special device is the one realized by Y. Chao et al. [42]. Although it is not a real MIMS structure (the emitter is not a metal) it is reviewed here because of the metal base. In the search for high frequency operation of polymer FETs, Y. Chao et al. proposed and fabricated the first organic THCT. The device has a common emitter current gain of 25 at room temperature. Unlike an earlier reported polymer metal base transistor [44], this device has no pinholes in the base, as confirmed with AFM. Because P3HT is not crystalline the quantum mechanical reflection at the base-collector interface will not happen in this transistor. This results in the very high transfer ratio. An even higher common emitter current gain for a polymer hot carrier device was reported by C. Chang et al.: 41 at room temperature.

Table 3 Parameters and performances of past MIMS's [1]

Emitter metal	E-B barrier material	E-B barrier thickness [Å]	Base metal	Base Thickness [Å]	Collector material	α_{max}	Reference
Au	Al_2O_3	Not given	Al	100	n-Ge	0.9	[5]
Hg	SiO	40	Au	100	n-Si	0.5	[20]
Pb	Al_2O_3	~30	Al	800	n-Ge	10^{-3}	[21]
Au	Al_2O_3	Not given	Al	150,800	n-Si	10^{-2},10^{-4}	[22]
PVK	LiF	28	Al	90	P3HT	0.96 (β=25)	[42]
Pentacene /NPB	LiF	7	Al	42	Pentacene /CuPC	0.98 (β=41)	[43]

4.1.3 MIMIM

The MIMIM transistor basically consists of a tunnel injector made with a metal-insulator-metal barrier and a collector, also made with a metal-insulator-metal barrier (Fig. 8).

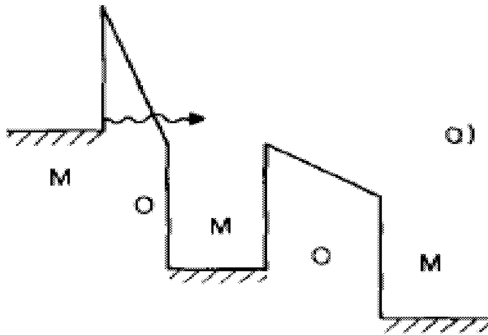

Fig. 8 Schematic band diagram of a MIMIM (here realized as a MOMOM). [9]

a) Design considerations

Heiblum has predicted the performance of a MIMIM amplifier. These calculations result in the requirement of a low Φ_E, thick d_{BE} emitter-base barrier [1]. In Fig. 9 results are plotted for different values of Φ_E, d_{BE} and L_o. L_o is a characteristic constant in the base metal: the mean free path of electrons with an excess energy of 1 eV.

The calculations were based on ideal structure, in practice difficulties are encountered (which are partly also applicable to other hot electron transistors):

-Non-tunneling current: transfer of electrons through pinholes and metallic microbridges in the barrier.

-Inelastic tunneling: interactions of electrons with resonance centers in the barriers.

-Barrier impurities and traps: imperfections change locally the barrier height which is especially important for the collector barrier. Traps will reduce the collected current.

-Base pinholes: electrons transfer through the base, without being affected by the base voltage.

-Base spreading resistance: the base spreading resistance should be much smaller than r_{in} to avoid V_{BE} being dependent on the base current. The spreading resistance increases when the base is made thinner

-Skin effects in the base: high frequency operation will lead to coupling between collector and emitter

-Interface states: interface states could act as trapping centers and reduce the transfer ratio.

-Geometrical realization of signal coupling: since the area of the devices are small, some kind of a high frequency signal concentrator (antenna) is needed to guide energy into the device.

b) Realized devices

The first MIMIM transistor was made by C.A. Mead [10] in 1960. This device was also the first tunneling hot carrier transistor ever. Mead used a metal-oxide-metal-oxide-metal (MOMOM) structure. The characteristics of previously produced devices are shown in Table 1.

The barrier height of a Al-Al_2O_3 barrier is about 2 eV. This means the electrons have to be injected in the base with an energy of at least 2 eV to be able to surmount the collector barrier. This high excess energy results in a high scattering. Another consequence is that the oxide layer of the emitter-base junction has to be thick to withstand voltages of V_{BE}>2V, which also reduces the transfer ratio. In [13], [14] the barrier height Φ_C was reduced to 0.7 eV. Also the electron-electron scattering mean free path was increased. As a result the transfer ratio of the device was higher.

W. Saitoh et al. reported the most recent MIMIM [15]. He used $CoSi_2$ and CaF_2 for the metal and the insulator respectively. Both materials have the fluorite lattice structure and are nearly lattice matched to Si, which results in layers with a minimized amount of defects. These high quality layers also increase the breakdown voltage of the insulating layers. Although Φ_E and Φ_C are the same and there is no graded collector barrier potential, the performance is very good.

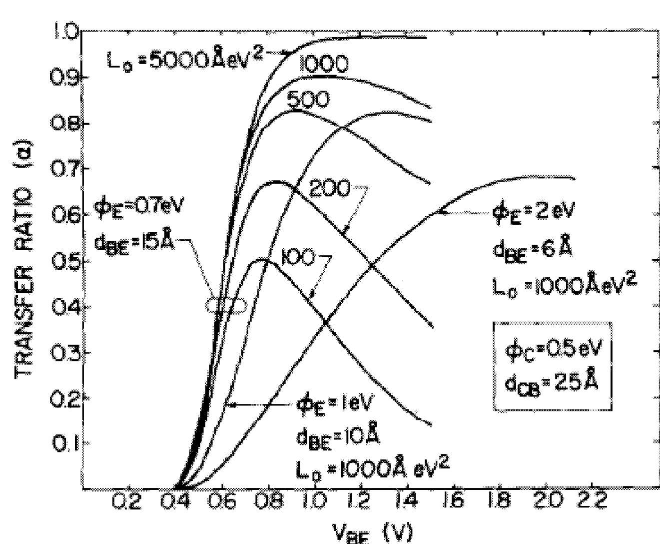

Fig. 9 Transfer characteristics of the model low Φ_E, thick d_{BE} MOMOM with L_o as a parameter. A comparison with a high Φ_E, thin d_{BE} is also plotted.

Table 4 Parameters and performances of past MIMIM's [1]

Emitter metal	E-B barrier	E-B barrier thickness [Å]	Base metal	Base Thickness [Å]	B-C barrier	B-C barrier thickness [Å]	Collector metal	α_{max}	Reference
Al	Al_2O_3	70	Al	100	SiO	100	Al	0.1	[10]
Al	Al_2O_3	40	Al	200	Al_2O_3	50	Al	0.02 (77K)	[11]
Al	Al_2O_3	33	Al	150	Al_2O_3	33	Al	0.01 (77K)	[12]
Al	Al_2O_3	100	Al	130,150	Al_2O_3	100	Al	.26, .2 (300K)	[13], [14]
$CoSi_2$	CaF_2	19	$CoSi_2$	19	CaF_2	50	n-Si (10^{22} cm^{-3})	0.94 (β=36)(77K)	[15]

4.1.4 Superconducting base HET (SBHET)

As a desert, the superconducting base hot electron transistor is introduced. In 1991 H. Abe et al. proposed to use a high T_c superconductor (HiTcSu) as the base material [26]. In Fig. 10 the energy band diagram of a device with a metal insulator hot electron injector is shown, a p-type HiTcSu and a n-type collector. Obviously, this device is very similar to a MIMS.

a) Design considerations

Abe et al. have performed theoretical calculations on the SBHET. They expect the device to exhibit a frequency performance around 400 GHz depending on the size of the emitter electrode and the width of the base.

The quantum mechanical reflection in the SBHET takes a minimum value when E_x' is slightly above the collector energy barrier Φ_C. This in contrast to a conventional metal base HET where the minimum occurs at E_x' far above the collector energy barrier. In a device with a semiconductor injector QMR as low as 0.05 are calculated.

The current gain as function of temperature is shown in Fig. 11 (look at MI-HET line).

A difficulty with these SBHETs is the growth of HiTcSus on semiconductors for the base collector interface. Abe et al. proposed to use a thin metal film to protect the semiconductor from oxidation.

b) Realized devices

The SBHET is only proposed by Abe et al., a real device has never been realized.

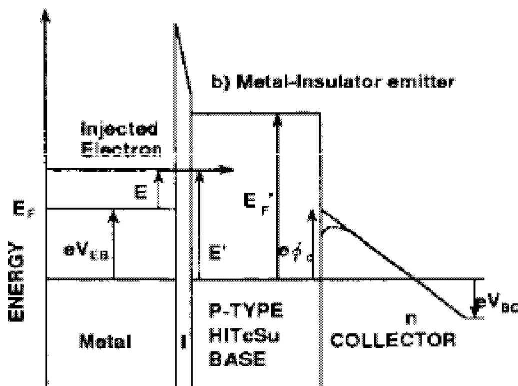

Fig. 10 Superconducting metal base tunneling hot electron transistor [26]

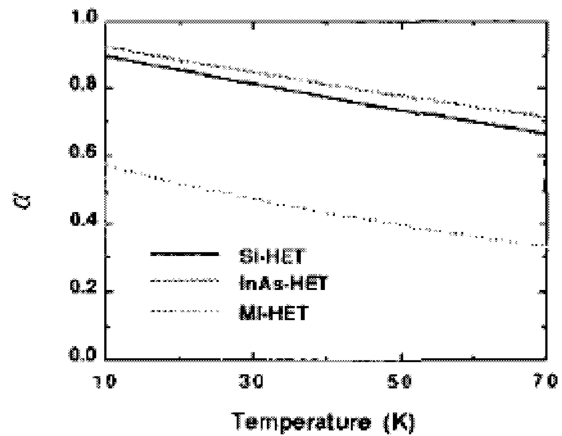

Fig. 11 Current gain of SBHETs as function of temperature [26]

4.2 Monolithic semiconductor

The failure of MIM-collector devices to exhibit a high transfer ratio has lead to a decrease of interest and an almost complete stop of research in the late 1960's.

Main difficulties are:

- -lattice mismatch
- -exposure to air in between layer-deposition
- -reflections from base collector interface

It is highly desirable to produce a device which consists entirely of semiconductors with approximately the same lattice constant. Advances in molecular beam epitaxy (MBE) semiconductor deposition techniques have enabled us to grow perfect semiconductor layers

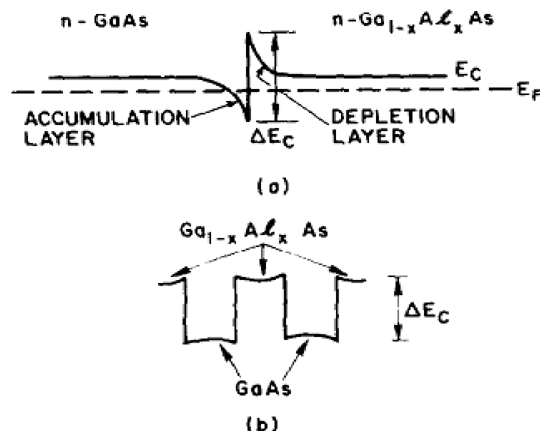

Fig. 12 Band diagrams of GaAs- $Ga_{1-x}Al_xAs$ heterojunctions [1]

on top of each other. So there are no problems with pinholes in the insulator layers. Besides this, we have the possibility to dope the semiconductor graded. This enables us to construct a graded base-collector barrier, which diminishes bases-collector reflections to a great extent and enhances the transfer ratio.

If two semiconductors are put in contact, a discontinuity in the energy band is created. For a GaAs-$Ga_{1-x}Al_xAs$ heterojunction, the discontinuity in the conduction band is shown in Fig. 12(a). When the layers are thinner than the depletion region of the accumulation layer a band scheme as in Fig. 12(b) is created.

4.2.1 THETA

The THETA (tunneling hot electron transfer amplifier) looks very much like a MIMIM, but is realized in semiconductor material like GaAs. In Fig. 13 the energy band diagram of the THETA with the highest current gain is shown.

In Heiblum's 1985 paper, he used the name THETA for all tunneling hot electron amplifiers, but later this name was especially reserved for heterojunction semiconductor tunneling hot electron amplifiers.

a) design considerations

In the eighties, heterojunctions of GaAs-$Ga_{1-x}Al_xAs$ and GaAs-Ge were well studied. The two layers had approximately the same lattice constant. Researchers chose for the first combination to realize their devices, because it was possible to change the barrier height of the junction by changing the value of x. Upon increasing the Al content GaAs changes from a direct gap to an indirect gap semiconductor and the bandgap changes from 1.43 to 2.1 eV. With this it is possible to change the barrier height from 0-0.4 eV.

For small ohmic contact, low spreading resistance and high base current saturation, the base has to be heavily doped, which in turn reduces the mean free path of the hot electrons due to impurity scattering. Heavy doping of the base can also be achieved by heavy doping of the GaAlAs layers. The electrons in these layers will spill over in the base that acts as an electron well. This approach doesn't have the disadvantage of introducing doping impurities. Although Heiblum has proposed this approach in [1], he didn't use it in the practical realization of the THETA [29],.

Even with a carrier concentration of 10^{20} cm^{-3} the base spreading resistance is still a few hundred ohms which requires the input resistance to be in the kilo-ohm range. Ultimately the base spreading resistance may also limit the frequency performance of the device.

After a lot of research of THETA's, Heiblum concludes that the Γ-L valley energy transfer is the most important energy loss mechanism. So the goal is to make the Γ-L energy separation in the base as large as possible.

A difficulty specifically arising for monolithic semiconductor HCTs is the contact of the signal lines with the semiconductor.

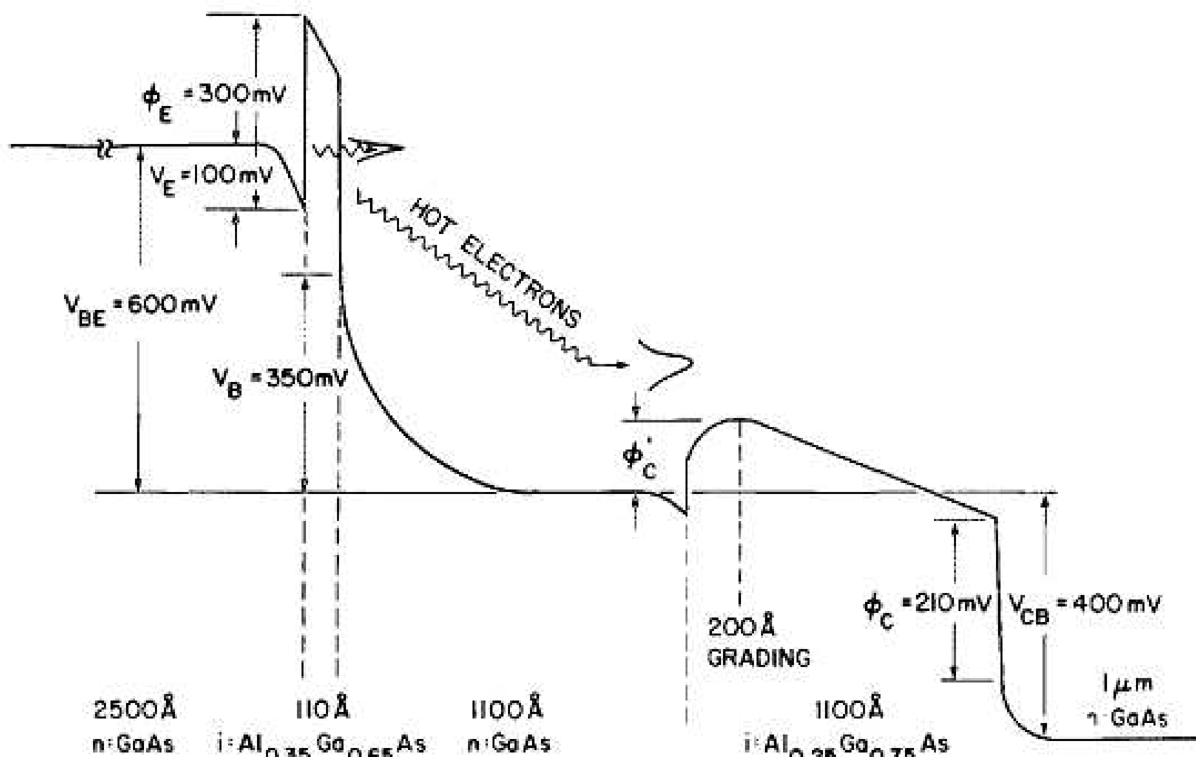

Fig. 13 Energy diagram of the THETA realized by Heiblum et al. with a current gain of 0.7 [29]

b) Realized devices

N. Yokoyama et al. were the first to report a working THETA in 1985, a year later Heiblum et al. published their device [29] that they further improved to get a maximum transfer ratio of 0.97 (common emitter current gain of 41). Results are summarized in Table 5. A schematic layout of the structure of Yokoyama's device is shown in Fig. 14.

The transfer ratio's of both devices were much higher than those observed for MOMOMs. First of all the layers had a much better quality, because of the matched lattice constants. Secondly, the barrier heights in the devices can be adjusted to the optimal value by changing the aluminum content.

Improvements in Heiblum's device were the graded basis-collector barrier to reduce quantum mechanical reflections and a lower doping in the base to reduce impurity and plasmon scattering. These improvements came at the cost of a lower output differential resistance: 150 kΩ for an abrupt junction device and 36 kΩ for a graded junction device [32].

By using a pseudomorphic base (making the base thinner), the transfer ratio and current gain could be further improved [30],[32]. In [30] a pseudomorphic InGaAs base is used that increases the $E_{\Gamma L}$ intervalley separation from 0.29 to 0.38 eV in comparison to a GaAs. A further improvement is the larger band discontinuity between InGaAs and AlGaAs. These two improvements allow for a lower mole fraction AlAs in the barriers and a wider energy window without excessive leakage currents.

Note that the devices did not show transistor action at room temperature. Heiblum reported that above 160K thermionic emission was dominant, but at temperatures below 160K tunneling [29].

In Heiblum's device an interesting effect was observed, namely that the transfer ratio and the energy distributions did not change with injected electron energy. It seems that electrons always thermalize to the same level.

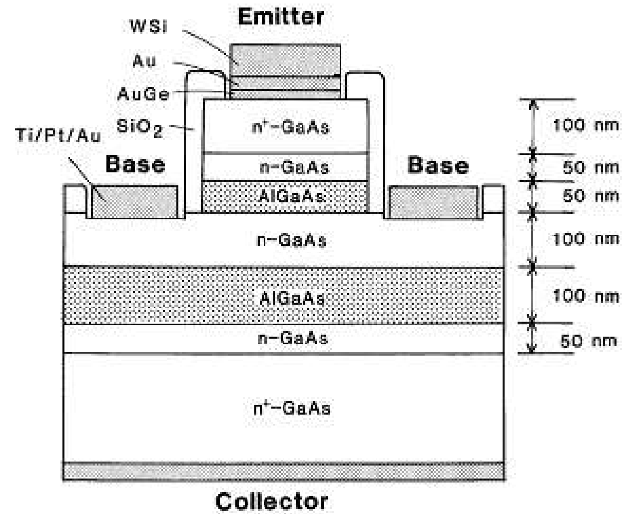

Fig. 14 Schematic cross section of a heterojunction tunneling hot electron transistor [27]

4.2.2 MI-p-n

This transistor has a MIS structure. The electrons tunnel from the metal emitter into the p-type base layer and the holes from the p-type base layer to the metal emitter. This makes the device bipolar, unlike the devices mentioned before (they are unipolar). The depletion layer between the p-type and n-type material functions as a collector barrier. A banddiagram of the device is shown in Fig. 15.

MI-p-n transistors are superior in gain, because the electrons injected in the base are very efficiently collected by the collector. The electrons can not thermalize below the collector potential barrier. Furthermore the base-collector leakage current is small allowing for use at room temperature.

a) Design considerations

The tunneling oxide is so thin that it does not impose any restrictions on electron current flows. It acts similarly to emitter resistance at higher current levels.

Table 5 Summary of parameters for realized THETA devices.

Emitter material	E-B barrier material	E-B barrier thick-ness [Å]	Base material	Base Thickness [Å]	B-C barrier material	B-C barrier thickness [Å]	Collector material [Å]	α_{max}	Refe-rence
n-GaAs	$Al_{0.7}Ga_{0.3}As$	500	n-GaAs	1000	$Al_{0.7}Ga_{0.3}As$	1000	n-GaAs	0.28 (β=0.38), 0.57 (40K)	[27], [28]
n-GaAs	$Al_{0.35}Ga_{0.65}As$	110	n-GaAs (2×10^{17} cm^{-3})	1100	Graded $Al_{0.25}Ga_{0.75}As$	1100	n-GaAs	0.7 (80K)	[29]
n-GaAs	$Al_{0.3}Ga_{0.57}As$	100	n-GaAs (7×10^{17} cm^{-3})	300	Graded $Al_{0.3}Ga_{0.57}As$	1000	n-GaAs	0.9 (4.2K)	[32]
n^+-GaAs	$Al_{0.28}Ga_{0.72}As$	100	n^+-$In_{0.12}Ga_{0.88}As$ (7×10^{17} cm^{-3})	210	Graded $Al_{0.1}Ga_{0.9}As$	650	$In_{0.12}Ga_{0.88}As$ / n^+-GaAs	0.97 (β=41) (77K)	[30]

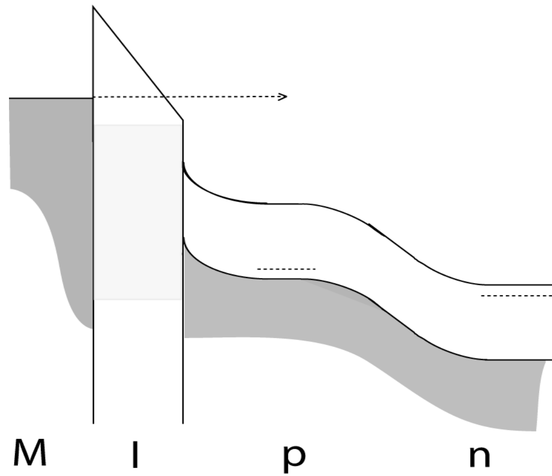

Fig. 15 Schematic banddiagram of the MI-p-n tunneling transistor.

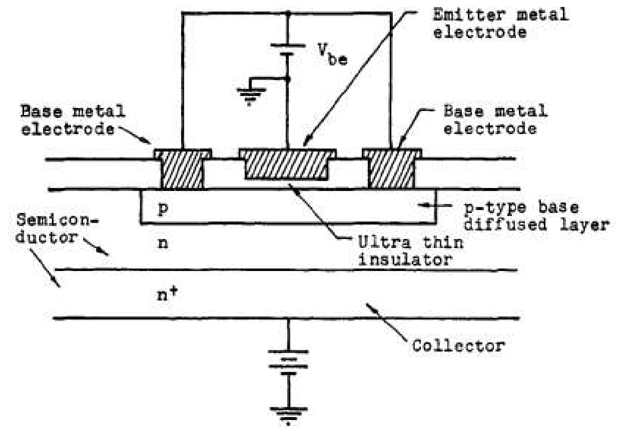

Fig. 16 Sketch of the MI-p-n transistor

The gain of the transistor is given by:

$$\beta = J_E / J_B = G_E \overline{D}_B / Q_B$$

G_E is the 'emitter Gummel number', a figure of merit for the emitter. D_B is the weighted average of the minority carrier diffusion coefficient within the base and Q_B is the integral of the doping density across the quasi neutral region of the base. For the transistor structure made by Green [34], Q_B is closely related to the implanted base dose.

This expression also explains the tradeoff involved between bipolar transistor gain and sensitivity to the effects of base-width modulation. Since small Q_B is required for large gain, the gain of a high-gain transistor will be more sensitive to changes in the charge associated with the collector base and hence the collector voltage.

b) Realized devices

H. Kisaki has made the first MI-p-n transistor [33]. A schematic layout of the device is shown in Fig. 16. He does not report any useful performance figures.

10 Years later M. A. Green manufactured a MI-p-n transistor with a common emitter gain approaching 25000 [34]. The structure is exactly the same as that of Kisaki. Both transistors have an emitter oxide layer of 20 Å. A difference is that Kisaki used diffusion doping for the base and Green ion implantation doping.

4.2.3 Resonant injector hot carrier transistors

A resonant injector is a double barrier quantum well structure that can improve the characteristics of any tunneling hot electron transistor.

The electrons are injected in the base by resonant tunneling through the discrete energy levels in the quantum well.

The operation principle of a resonant hot electron transistor is shown in Fig. 17. (A)If there is no emitter bias applied, no tunneling current occurs. (B) If the base emitter voltage is about $2E_1/q$ (E_1 is the first energy level in the quantum well) resonant tunneling occurs. (C) The base emitter bias is further increased and the collector current decreases, because there are less electrons tunneling (the fermi level of the emitter is not anymore aligned with the E_1 level of the quantum well).

The main advantage of a resonant injector is the reduced width of the energy distribution of the tunneling electrons. But there is also another benefit from the resonant injector. It has a more pronounced negative differential resistance effect than a normal, single barrier injector due to the quantization of energy levels in the space between the barriers. A sharp drop in current can be seen in Fig. 18. This current drop is quantified by the peak to valley ratio (PVR). Because of the higher PVR than normal tunneling transistors, resonant injector devices are better suited for electronics circuits that exploit the NDR effect of tunneling transistors like an exclusive NOR gate with a single transistor [40].

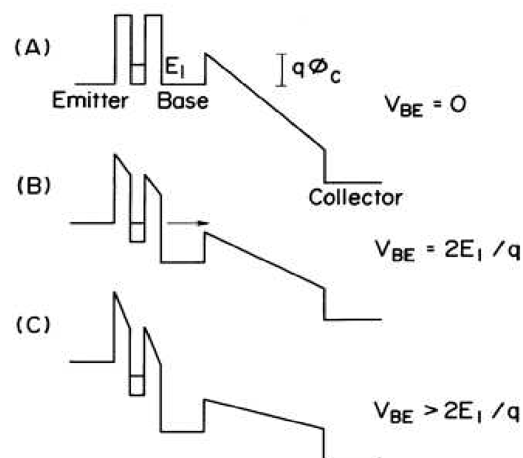

Fig. 17 Operation principle of a resonant hot electron transistor [35]

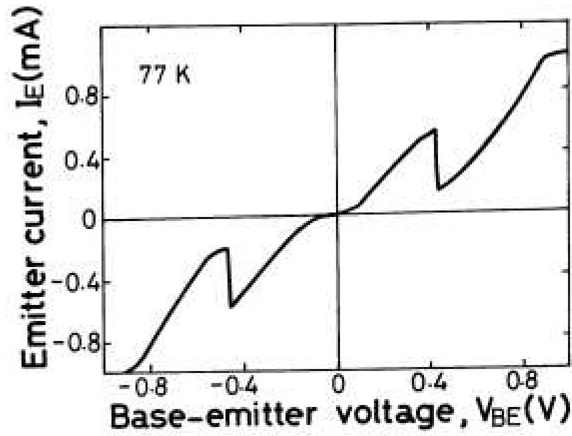

Fig. 18 Base emitter I-V characteristics of a RHET measured at 77K [35].

a) Design considerations

As was mentioned before, the PVR is very important in resonant tunneling devices. For practical application, the RHET must have a PVR of at least 10 and a peak current density of 10^5 A cm^{-2} at 77K [45]. To achieve a high PVR, asymmetric barriers can be used. This modification increases the overall transmission coefficient and decreases the thermionic emission current over the base side barrier. This has positive effects on respectively the peak current and the valley current.

There are many new theoretical phenomena occurring in resonant tunneling injector hot carrier transistors. In this paper, only the most important characteristics of the resonant injector are mentioned. For extensive theoretical descriptions I want to refer to [47] and [48].

b) Realized devices

The first RHET (resonant hot electron transistor) was fabricated in 1985 by N. Yokoyama et al. [40] This transistor is an improvement of a THETA by adding a resonant tunneling injector. A year later a better version of the device was published [36]. This RHET has an asymmetric resonant tunneling barrier (see Fig. 20) to increase the PVR.

Imamura et al. compared a RHET with a InGaAs base with a RHET with an InAs base [38]. Due to the larger Γ-L valley separation (1.05 eV for InAs and 0.55 eV for InGaAs) and the lower effective electron mass (0.023 for InAs and 0.042 InGaAs) the InAs base device performs better than the other. To reduce strain in the base, two thin layers of InGaAs have been introduced. This article is one of the few that publishes data about the frequency performance of THCTs. At a temperature in the range of 50 to 80 K a current gain cut-off frequency of 64 GHz and a maximum oscillation frequency of 50 GHz were measured. In an article published a year before, a current gain cut-off frequency of 121 GHz at a temperature below 77K and at a current density of 6.7×10^4 A/cm^2 was reported [49]

The publication of J. Chen et al. [39] uses a quantum well as replacement for the base in a conventional HCT, therefore I refer to the well as the 'base'. In this device the 'base' is not directly contacted by an ohmic contact, but tunneling is used to change its potential, very much like the operating principle of a SET (single electron transistor). The quantum well nature of the 'base' results in a very narrow energy spreading of the

Table 6 Summary of parameters for realized THETA devices.

Emitter material	Injector materials	Injector dimensions [Å] (Barrier/well/barrier)	Base material	Base Thickness [Å]	B-C barrier material	B-C barrier thickness [Å]	Collector material [Å]	α_{max}	Peak to valley ratio (PVR)	Reference
n^+-GaAs	$Al_{0.33}Ga_{0.67}As$/GaAs/ $Al_{0.33}Ga_{0.67}As$	50/56/50	n^+-GaAs	1000	$Al_{0.2}Ga_{0.8}As$	3000	n^+-GaAs	-	-	[40]
n^+-GaAs	$Al_{0.3}Ga_{0.7}As$/ GaAs/ $Al_{0.53}Ga_{0.47}As$	50.9/36.8/31.1	n^+-GaAs	250	$Al_{0.16}Ga_{0.84}As$ (graded)	3000	n^+-GaAs	0.84 (β=5) (77K)	2.6 (77K)	[36]
n-InGaAs	$In_{0.52}Al_{0.48}As$/$In_{0.53}Ga_{0.47}As$/ $In_{0.52}Al_{0.48}As$	25.5/41/25.5	n-InGaAs	300	$In_{0.52}(Al_{0.5}Ga_{0.5})_{0.48}As$	2000	n-InGaAs	0.85 (β=4) (40K)	-	[38]
n-InGaAs	$In_{0.52}Al_{0.48}As$/$In_{0.53}Ga_{0.47}As$/ $In_{0.52}Al_{0.48}As$	25.5/41/25.5	n-InAs/n-InGaAs/InAs/n-InGaAs/InAs	93/10/93/10/93	$In_{0.52}(Al_xGa_{1-x})_{0.48}As$ (x=0.25,0.33, 0.5)	400/1000/600	n-InGaAs	0.96 (β=8) (40K)	-	[38]
n^+-GaAs	$Al_{0.4}Ga_{0.6}As$/ GaAs/ $Al_{0.4}Ga_{0.6}As$	30/100/30	n^+GaAs	100	$Al_{0.4}Ga_{0.6}As$	3000	n^+-GaAs	0.95 (β=1.2) (77K)	35 (77K)	[39]
$CoSi_2$	CaF_2	9	$CoSi_2$	16	CaF_2/ $CoSi_2$/ CaF_2	9/22/9	n-Si	0.99 (77K) (est.)	~10 (300K)	[47]
n-AlGaAs (see Fig. 19)	AlAs/GaAs/ AlAs	20/50/20	p^+-GaAs	2000	-	-	n-GaAs	0.95 (β=20) (77K)	1.8 (77K)	[37]

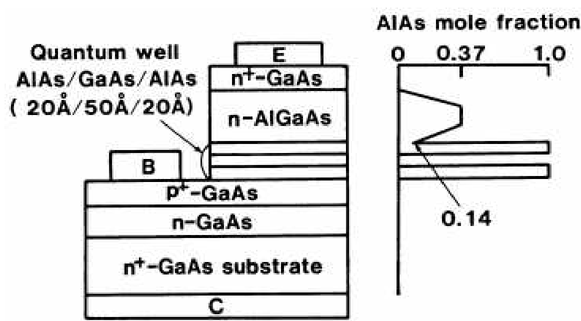

Fig. 19 Schematic cross section and composition of the resonant bipolar transistor [37]

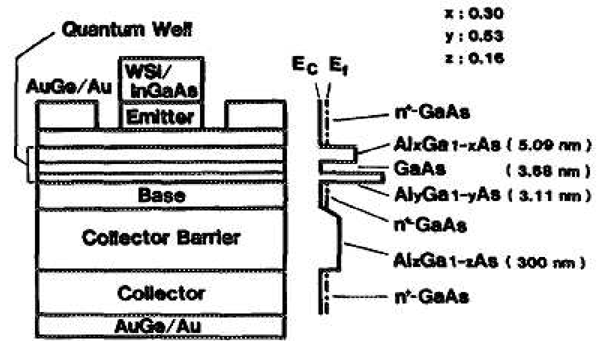

Fig. 20 Schematic layout and bandstructure of an asymmetric barrier RHET [36

hot electrons. This narrow spread has a positive effect on the PVR, which is 35 and in one special case even as large as 4691. The high transfer ratio is inconsistent with the common emitter current gain of ~1.2, because of the complexity in hot electron transport and the way energy bands bend in response to biases. Effects especially important for this thin 'base' device.

In 1995, the first metal-insulator resonant hot electron transistor was fabricated [47]. Although this is the chapter with monolithic semiconductor devices, the device is reviewed here. This MI RHET has a structure that is even more special than the device with the quantum well base: the collector barrier is a quantum well resonant tunneling structure and the base is so thin that it is a quantum well too. The emitter-base barrier is a normal, single barrier. The overall structure thickness is very low and the quality of the films is high, so the estimated transfer efficiency is very high at 0.99. The thin collector barriers and parasitic effects caused by the SiO_2 layer covering the device cause degradation of performance. Nevertheless, at room temperature a high PVR and transistor action were observed.

Not only the THETA and the MIMIM can be improved by adding a resonant injector, also the MI-p-n [37]. By doing that, it is possible to make a resonant tunneling bipolar hot carrier device. Resonant tunneling of holes was observed and studied in this device.

5 Conclusion

The idea of a tunneling hot carrier transistor is already very old, as C.A. Mead proposed and manufactured the first in 1960. Although the frequency performance prospects seemed very good, not an overwhelmingly large amount of research into THCTs has been done. The major causes for this lack of interest were the disappointing transfer ratios and the fast developments in rival pn-junction bipolar transistors.

The disappointing performance of metal base THCTs was first appointed to the reflections from the base-collector barrier, but the $CoSi_2$-CaF_2 MIMIM proves the contrary. Although this device has almost square barriers, the transfer ratio is very high, due to the good quality of the insulating CaF_2 films. So, the low transfer ratio of the metal base THCTs was probably due to the bad quality of the oxide insulating layers. Still, the main loss mechanism in a MI-THCT with good barriers could be the reflections from the base-collector barrier.

Monolithic semiconductor base devices have a much higher transfer ratio than most metal base devices. Again, this is mainly because of the good quality of the layers. With pseudomorphic layers, the transfer ratio of the devices was even higher. A second advantage of the monolithic semiconductor base devices is the low effective mass of the hot electrons, which makes them go faster. Thirdly, the control over the Al fraction in the AlGaAs greatly enhances the design flexibility of the devices. For example a graded base-collector can be made to reduce reflection effects. The main problem of monolithic semiconductor base THCTs is the intervalley scattering. Attempts have been made to enlarge the Γ-L separation by using an InGaAs base.

To improve the transfer efficiency of hot electrons and enhance the negative differential effect for use in logic circuit applications, a double barrier quantum well replaced emitter-base barrier. This modification resulted in good performing devices with possible applications in logic circuits.

The problem with nearly all THCTs is their limited operating temperature range. Almost all fabricated devices show reasonable performances at ~80K. Nevertheless, the low operating temperature range is an advantage over the conventional doped semiconductor electronics for applications in low temperature environments like outer space. Because the barriers in GaAs-AlGaAs cannot be made higher than 0.4 eV, there is no prospect for operation at room temperature. Much higher barriers are needed. Promising devices in this aspect are the $CoSi_2$-CaF_2 metal insulator RHET, the MI-pn by M.A. Green and the organic MIMSs, these have all shown transistor action at room temperature.

The results of both the $CoSi_2$-CaF_2 RHET and the $CoSi_2$-CaF_2 MIMIM are promising. The devices have very high transfer ratios although they don't have graded collector barriers. The possibility to operate at higher temperatures is not the only advantage of MI structures over heterojunction semiconductor structures. The higher carrier concentration and lower resistivity of metals contribute to the reduction of device

size (the thickness of MI devices is an order of magnitude smaller than the thickness semiconductor devices), high current density, less problems with base spreading resistance and less lead resistance. The low dielectric constant of the insulator decreases the capacitance and thereby decreases the response time of the device.

Frequency performance data are published only for monolithic semiconductor base devices. Although they are not yet in the THz range, at 121 GHz, they are still promising. A corporation, Phiar [50], is expecting to be able to produce THCTs at 3 THz by 2010. Phiar recently [50] proposed a new structure, the MIIMIM. With this double insulator electron injector, a RHET with an induced quantum well is fabricated.

Another new development in the area of THCTs are the polymer hot carrier MIMS structure transistors with a very high common emitter current gain at room temperature. Because the polymers are not crystalline, the base-collector interface is 'soft' and there is almost no reflection from the barrier. These results suggest that future research on THCTs should focus more on the use of organic materials.

6 Acknowledgements

I wish to thank Dr. B. de Boer for the good supervision and useful discussions and Drs. A.J. Kronemeijer also for the useful discussions.

7 References

1. M. Heiblum, Solid state electronics **24**, 343 (1981)
2. M. Heiblum, M. V. Fischetti, IBM J. Res. Develop. **34**, 530 (1990)
3. M. Heiblum, M. V. Fischetti, W. P. Dumke, D. J. Frank, I. M Anderson, C. M. Knoedler, and L. Osterling, Phys. Rev. Lett. **58**, 816 (1987)
4. A. F. J. Levi, J. R. Hayes, P. M. Platzman, and W. Wiegmann, Phys. Rev. Lett. **55**, 2071 (1985)
5. J.P. Spratt, R.F. Schwarz, W.M. Kane, Phys. Rev. Lett. **6**, 341 (1961)
6. A. F. J. Levi, J. R. Hayes, P. M. Platzman, and W. Weigman, Phys. B **134**, 4801 (1985)
7. M.A. Hollis, S.A. Palmateer, L. F. Eastman, N. V. Dandekar, and P. M. Smith, IEEE Electron Device Lett. EDL-**4**, 440 (1983)
8. S. M. Sze, C. R. Crowel, G. P. Carey and E. E. LaBate, J. Appl. Phys. **37**, 2690 (1966)
9. S. Luryi, A. Kastalsky, Physica **134B**, 453 (1985)
10. C.A. Mead, J. Appl. Phys. **32**, 646 (1961)
11. O. L. Nelson and D. E. Anderson, J. Appl. Phys. **37**, 66 (1964)
12. E. E. Huber, Jr., F. E. Johnston, Jr. and C. K. Kirk, Jr., J. Appl. Phys. **39**, 5104 (1968)
13. J. Antula, J. Appl Phys. **43**, 1830 (1972)
14. J. Antula, Thin Solid Films **13**, 93 (1972)
15. W. Saitoh, T. Suemasu, Y. Kohno, M. Watanabe, M. Asada, Jpn. J. Appl. Phys. **34**, L1254 (1995)
16. J. Cohen, 1 Appl. Phys. **33**, 1999 (1962)
17. J. Cohen, Appl. Phys. Lett. **1**, 61 (1962)
18. H. Hanter and W. A. Feibelman, J. Appl. Phys. **33**, 3580 (1962)
19. W. Hess and R. Johannes, Brit. J. Appl Phys. **14**, 287 (1963)
20. D. Kahng, Proc. IRE **50**, 1534 (1962)
21. C. Guinet, Appl. Phys. Lett. **25**, 600 (1974)
22. W. Ludwig, G. V. Reinsperger and W. Gericke, Thin Solid Films **36**, 415 (1975)
23. D. J. E. Knight and P. T. Woods, J. Phys. E **9**, 898 (1976)
24. J. J. Jimenez and R. Petersen, Infrared Phys. **17**, 541 (1977)
25. C. R. Crowel and S. M. Sze, J. Appl. Phys. **37**, 2683 (1966)
26. H Abe, T Yamada, M Oglwara, T Tsuruoka, K Hasimoto, R Kawasaki, Supercond. Sci. Technol. **4**, 598 (1991)
27. N. Yokoyama, K. Imamura, T. Ohshima, H. Nishi, S. Muto, K. Kondo, S. Hiyamizu, Jap. J. Appl Phys. **23**, L311 (1984)
28. N. Yokoyama, K. Imamura, T. Ohshima, H. Nishi, S. Muto, K. Kondo, S. Hiyamizu, Technical digest of IEDM (IEDM, San Francisco, CA, 1984), p. 532
29. M. Heiblum, D.C. Thomas, C.M. Knoedler, M.I. Nathan, Appl. Phys. Lett. **47**, 1105 (1985)
30. K. Seo M. Heiblum, C.M. Knoedler, J.E. Oh, J. Pamulapati, P. Bhattacharya, IEEE Electron device letters **10**, 73 (1989)
31. Y. Miyamoto, R. Nagakawa, I. Kashima, M. Ishida, N. Machida, K. Furuya, IEICE Trans. Eectron. **E89–C**, 972 (2006)
32. M. Heiblum, I.M. Anderson, C.M. Knoedler, Appl. phys. lett. **49**, 207 (1986)
33. H. Kisaki, IEEE proc. lett. **61**,1053 (1973)
34. M.A. Green, R.B. Godfrey, IEEE electron dev. lett. **4**, 225 (1983)
35. N. Yokoyama, K. Imamura, S. Muto, S. Hiyamizu, H. Nishi, Japan. J. Appl. Phys. **24**, L853 (1985)
36. T. Mori, H. Onishi, K. Imamura, S. Muto, N. Yokoyama, Appl. Phys. Lett. **49**, 1779 (1986)
37. T. Futatsugi, Y. Yamaguchi, K. Imamura, S. Muto, N. Yokoyama, A. Shibatomi, Jap. J. Appl. Phys. **26**, L131 (1987)
38. K. Imamura, T. Adachihara, T. Mori, S. Muto, N. Yokoyama, IEEE Trans. Electron Dev. **39**, 479 (1992)
39. J. Chen, C. Yang, R.A. Wilson, IEEE Trans. Electron Dev. **40**, 267 (1993)
40. G.I. Haddad, P.Mazumder, Solid state electronics **41**, 1515 (1997)
41. T. C. L. G. Sollner, W. D. Goodhue, P. E. Tannenwald, C. D. Parker, and D. D. Peck, Appl. Phys. Lett. **43**, 588 (1983)
42. Y. Chao, S. Yang, H. Meng, Appl. Phys. Lett. **87**, 253508 (2005)
43. C. Yang, T. Ou, S. Cheng, M. Wu, S. Lin, Y. Chan, Appl. Phys. Lett. **90**, 153509 (2007)
44. M.S. Meruvia, A.R.V. Benvenho, I.A. Hümmelgen, A.A. Pasa, W. Schwarzacher, Appl. Phys. Lett. **86**, 263504 (2005)
45. S. Muto, T. Inata, Semic. Sci. Technology **9**, 1157 (1994)
46. Brown ER. Sonderstrom I R, Parker C D, Mahoney L I, Molvar K M and McGill T C 1991 Appl, Phys. Lett. **58**, 2291
47. T. Suemasu, Y. Kohno, W. Saitoh, M. Watanabe, and M. Asada, IEEE Trans. Electron. Dev. **42**, 2203 (1995)
48. H. Sheng, S. Chua, Semicond. Sci. Techn. **8**, 1590 (1993)
49. T. Mori, T. Adachihara, M. Takatsu, H. Ohnishi, K. Imamura, S. Muto and N. Yokoyama, Electron Lett. **27**, 1523 (1991).
50. http://www.phiar.com/transistors.php4
51. D. Lacour, M. Hehn, F. Montaigne, H. Jaffres, P. Rottlander, G. Rodary, F. Nguyen Van Dau, F. Petroff, A. Schuhl, Europhys. Lett. **60**, 896 (2002)

8 Appendix A

Mean free path data for different excess energies in different materials [1]

Material	Excess Energy [eV]	Mean Free Path [Å]	Reference
Al	0.7	~100	55
	0.9	~200	52
	1	~100	52
	1	60	54
	1.5	~50	52
	1.5-1.85	90	66
	2	150	49
	2.5	$\ell_{e-e}\sim 220$	53
	2-3	130	52
	3	300	73
	4	70+10	31
	5	$\ell_{e-e}\sim 50, \ell_i\sim 250$	62
	6	50±10	31
	6-7	75	47
	9	$\ell_{e-e}\sim 510, \ell_{e-ph}\sim 130$	63
Pd	1	$\ell_{e-e}\sim 650$, $\ell_{e-ph}\sim 110$	55
	1.1	170	57,61
Cr	2.8	35	59
Cu	0.55	430	36
	0.927	70-110	69
	1.1	50-200	57,61
K	[illegible]	1000	58
Au	0.8	55±100(holes)	68
	0.85	520±5	70
	0.95	350	60
	1	700	71
	1	$\ell_{e-e}\sim 1200$, $\ell_{e-ph}\sim 406$	55
	1.1	740	57,61
	1.1	740	72
	2	$\ell_{e-e}\sim 140$	64
	2	200	71
	3	$\ell_{e-e}\sim 120$	64
	3.2	70	59
	4	$\ell_{e-e}\sim 50$	64
	5	$\ell_{e-e}\sim 50$	64
	5	70	71
	7	80	46
	7	47	48
	7	57	50
	7-10	180	46
	5.5-10	$\ell_{e-e}<45$, $\ell_{e-ph}\sim 250$	62
	12	400-600	67
Ag	0.65	370	36
	1	$\ell_{e-e}\sim 1100$, $\ell_{e-ph}\sim 570$	55
	1.1	440	57,61
Material	Excess Energy [eV]	Mean Free Path [Å]	Reference
	1.9	200-300	51
	5	48	51
	5.5	70	56
	5.5-8	$\ell_{e-e}<42$, $\ell_{e-ph}\sim 400$	62
	12	250-700	67
In	4.27	42	65
	4.9	30.5	65
	5.65	18.5	65